



**Unusual magnetic damping effect in silver-cobalt ferrite  
hetero nano-system**

Journal:	<i>RSC Advances</i>
Manuscript ID:	RA-COM-11-2014-014960.R2
Article Type:	Communication
Date Submitted by the Author:	26-Jan-2015
Complete List of Authors:	<p>Sharma, Surender; Université Paris Diderot, ITODYS  Vargas, Jose; Advanced Materials Research Institute, University of New Orleans,  Vargas, Nicolas; Physics Department, Universidad de Santiago de Chile and CEDENNA, USACH,,  Sepúlveda, Sebastian; Physics Department, Universidad de Santiago de Chile and CEDENNA, USACH,,  Altbir, Dora; Physics Department, Universidad de Santiago de Chile and CEDENNA, USACH,,  Pirota, Kleber; Instituto de Fisica Gleb Wataghin, Universidade Estadual de Campinas (UNICAMP) Campinas, 13.083-859,  Zboril, Radek; Regional Centre of Advanced Technologies and Materials, Zoppellaro, Giorgio; Regional Centre of Advanced Technologies and Materials, ; University of Oslo, IMBV  Knobel, Marcelo; Instituto de Fisica Gleb Wataghin, Universidade Estadual de Campinas (UNICAMP) Campinas, 13.083-859,</p>

## COMMUNICATION

## Unusual magnetic damping effect in silver-cobalt ferrite hetero nano-system

Cite this: DOI: 10.1039/x0xx00000x

Surender K. Sharma,<sup>1, 2, 3</sup> Jose Marcelo Vargas,<sup>4</sup> Nicolás Manuel Vargas,<sup>5</sup> Sebastian Castillo-Sepúlveda, Dora Altbir,<sup>5</sup> Kleber Roberto Pirota,<sup>1</sup> Radek Zboril,<sup>3</sup> Giorgio Zoppellaro,<sup>3</sup> and Marcelo Knobel<sup>1</sup>

Received 00th January 2012,  
Accepted 00th January 2012

DOI: 10.1039/x0xx00000x

www.rsc.org/

**The static and dynamic magnetic response of the newly synthesized CoFe<sub>2</sub>O<sub>4</sub>-Ag hetero nano-system showed significant enhancement in the effective energy barrier and reduction of the magnetic hardness of CoFe<sub>2</sub>O<sub>4</sub> upon interaction with non-magnetic Ag as compared to neat CoFe<sub>2</sub>O<sub>4</sub>. The observed magnetic properties of CoFe<sub>2</sub>O<sub>4</sub>-Ag have been dissected in detail using the superparamagnetic Stoner-Wohlfarth and Neel-Arrhenius/Vogel-Fulcher models with the aid of micromagnetic simulations.**

Hetero magnetic nanostructures are a class of nano-sized materials characterized by building constituents that differ from each other in shape, size and/or chemical nature. The diverse units are joined together by virtue of covalent bonds or electrostatic forces. The current research effort in the designs of hetero nanostructures aims to combine the electronic properties of different components in way to encode novel functions in the formed materials. Many examples of hetero-nanosystems can be found in literature, such as magneto-optical devices, nanocarriers/contrast agents used in biomedicine and red-ox components active in environmental bioremediation.<sup>1-3</sup> In the majority of the cases reported in literature, hetero-nanostructures have been synthesized easily from bottom-up approaches using, for example, preformed powdered components either through ball-milling processes or *via* cold-press mechanical assembly<sup>4</sup>. Besides mixing solid precursors, alternative synthetic routes have been explored, using fluid mixture of two components<sup>5</sup>, epitaxial nucleation/growth on preformed nano-seeds or thermal treatments followed by decomposition of core-shell nanoparticles<sup>6</sup>. Silver and Gold nanoparticles play important roles in many different areas. For example, they can serve as a model system to experimentally probe the effects of quantum confinement on electronic, magnetic, and other related properties. They have also been widely exploited for use in photography, catalysis, biological labeling, photonics, optoelectronics, information storage, and formulation of magnetic ferrofluids.<sup>7,8</sup> Examples of nanomaterials found in literature obtained via the latter routes are Ag-Fe<sub>3</sub>O<sub>4</sub><sup>9</sup>, Fe<sub>3</sub>O<sub>4</sub>/ZnSe<sup>10</sup> and Ag-CoFe<sub>2</sub>O<sub>4</sub>

heteromixtures.<sup>11</sup> Following the fluid-route pathway, in this work we report formation of the hetero nanocomposite CoFe<sub>2</sub>O<sub>4</sub>-Ag, coded hereafter CFO-Ag, system in which the metallic Ag nanoparticles have been assembled within the CoFe<sub>2</sub>O<sub>4</sub> material by using an *in-situ* synthetic approach. We demonstrate that in CFO-Ag the electronic interactions between the two different domains, non-magnetic Ag and magnetic CoFe<sub>2</sub>O<sub>4</sub> nanoparticles (coded thereafter CFO), can severely alter the magnetic relaxation behaviour of CFO, even though the relative concentration of Ag was kept low compared to the bulk CoFe<sub>2</sub>O<sub>4</sub>. Synthesis of the CFO-Ag hetero-system was carried out in two steps. Initially, CoFe<sub>2</sub>O<sub>4</sub> NPs with sizes of ~10-11 nm were obtained by thermal decomposition of Fe(acac)<sub>3</sub> (2.0 mmol) and Co(acac)<sub>3</sub> (1.0 mmol) in the presence of 1,2-hexadecanediol.<sup>9-11</sup> Then, an excess of the so-formed CoFe<sub>2</sub>O<sub>4</sub> NPs (25 mg) dispersed in oleylamine and oleic acid were used as seeds to grow Ag nanoparticles, starting from previously prepared Ag metallic precursor (C<sub>54</sub>H<sub>45</sub>NO<sub>3</sub>P<sub>3</sub>Ag, 5 mg of Ag),<sup>9</sup> and employing temperature gradients as the driving forces in the assembly process (100°C for 30 minutes, then 200°C for 60 minutes and finally 265°C for 120 minutes under argon atmosphere).

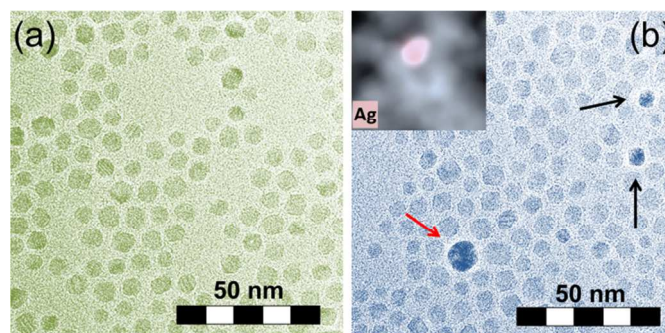


**Fig. 1.** (a) HRTEM images of neat CFO and (b) CFO-Ag NPs. In panel, (b) arrows indicate the metal Ag nanoparticles. The inset in

(b) shows the electron energy loss spectroscopy (EELS-TEM) with the chemical mapping (Ag) of CFO-Ag recorded around the Ag NPs region highlighted with the red-arrow.

The followed synthetic pathway allowed formation of metallic Ag nanoparticles inside the pool of CFO NPs, acting here as matrix. Further details of these synthetic steps are provided in the ESI file. The material composition, NPs sizes and crystallinity of CFO-Ag have been thoroughly screened by *X*-ray powder diffraction (XRD, ESI Fig. S1) and small-angle *X*-ray scattering analysis (SAXS, ESI Fig. S2) as well as low temperature (77 K) Mössbauer spectroscopy (ESI, Fig. S3 and Table S1). The results confirmed that during the *in-situ* synthesis of CFO-Ag no degradation of the  $\text{CoFe}_2\text{O}_4$  spinel ferrite phase occurred, as well as alteration of the original  $\text{CoFe}_2\text{O}_4$  mean particle size. Furthermore, these results validated the successful formation of metallic Ag nanoparticles. The morphological organization of the formed hetero nanosystem, CFO-Ag, was probed by TEM technique. The high-resolution micrograph obtained from transmission electron microscopy (HRTEM) is shown in Fig. 1b together with neat CFO NPs (Fig. 1a). Since both Ag and CFO NPs were surface functionalized by organic molecules of oleic acid, the presence of the organic canopy prevented the direct particle contacts. The relevant morphological data as obtained from TEM, SAXS and XRD measurements are collected together in Table 1 (upper part of the Table). From the TEM analyses, statistically only few CFO NPs were located close to the Ag NPs, while the majority of CFO nanoparticles fall more distant from the metallic Ag cores. Thus, CFO and Ag units forms in the hetero-nanosystem architectures that can be envisioned as locally organized in cores, which are made by those CFO located closer to Ag, surrounded by shells, the CFO matrix in which CFO fall far from Ag. Such morphological organization of CFO-Ag may promote the occurrence of electronic interactions in the portion of material where the CFO surfaces are closer to non-magnetic Ag, interactions that should affect the magnetic dynamics of the CFO surface atoms. Thus, the static and dynamic (dc and ac) magnetic behaviour of CFO-Ag and neat CFO have been recorded in order to reveal, if any, the electronic differences between hetero-composite and neat CFO material. Fig. 2a shows superimposed the recorded trends of the magnetization ( $M$ ) versus temperature ( $T$ ) in the zero-field-cooled (ZFC) and field-cooled (FC) for neat CFO and CFO-Ag. The low field  $M_{ZFC-FC}$  curves for CFO (Fig. 2a, green circles) exhibited a blocking process typical for ensembles of interacting and randomly oriented NPs. The observed maximum in  $M_{ZFC}$ , at  $T = 270$  K, is associated with the mean blocking temperature  $\langle T_B \rangle$  of superparamagnetic (SPM) particles. The observed increase of  $M_{FC}$  upon decreasing the temperature (below  $\langle T_B \rangle$ ) provided the first qualitative indication of the effectiveness of magnetic interparticle interactions, which is for CFO moderately dipolar. The result is in harmony with the presence of the organic capping that prevented in CFO the direct nanoparticle contacts, as already observed in the HRTEM micrographs shown earlier (Fig. 1a). Therefore, the magnetic signature witnessed in CFO followed the behaviour expected for a narrow distribution of magnetic mono domains with large magnetocrystalline anisotropy, as anticipated from the Stoner-Wohlfarth model.<sup>12</sup> When the CFO-Ag architecture was probed (Figure 2a, blue circles), the  $M$  vs.  $T$

$ZFC/FC$  responses followed trends comparable to those recorded for CFO, but displayed a clear decrease in  $\langle T_B \rangle$ , down to 250 K (see also Table 1, lower part). These data validated further the successful growth of the Ag NPs within the CFO matrix without promoting degradation and/or alteration of the mean CFO particle size; in fact, it is important to note that the  $M_{ZFC-FC}$  behaviours are very sensitive indicators to screen for changes in the magnetocrystalline anisotropy and/or particle size distribution. Comparing the  $T$ -variation of the magnetization in  $ZFC-FC$  protocol of CFO and CFO-Ag, the strong interparticle interaction seems to be not much affected. However, a small shift in  $T_B$  toward lower- $T$  can be addressed to the presence of smaller particles, as it clearly evident from the appearance of a doublet from low temperature (77 K) Mössbauer spectroscopy (ESI, Fig. S3). Fig. 2b illustrates the hysteresis loops recorded at 50 K for CFO and CFO-Ag. Differing from CFO (Fig. 2b, green circles), the hetero nano-system exhibited an anomaly in the hysteresis cycle in the low-field region (Fig. 2b, blue circles). The anomaly has been highlighted by broken-lines in Fig. 2b where a sharp drop of the magnetization occurred near to zero-field.

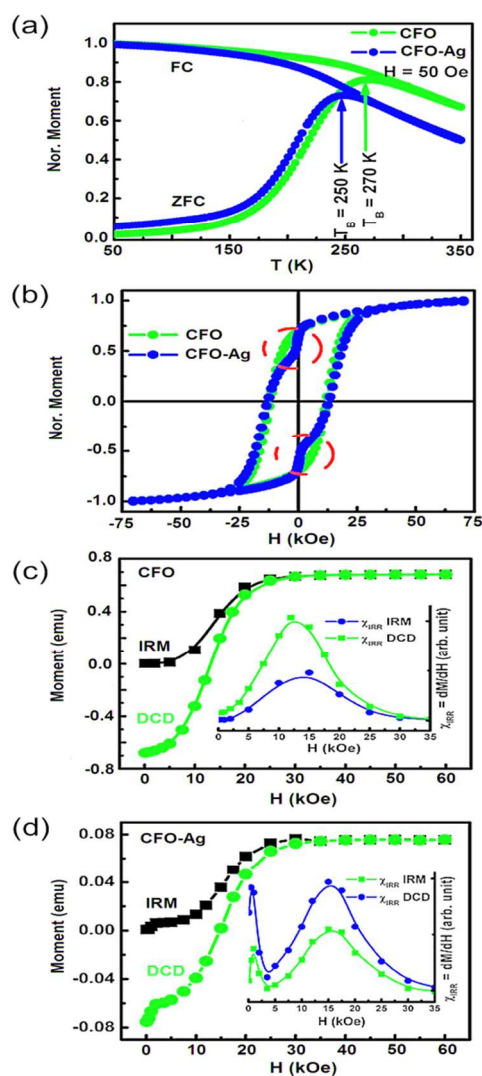


**Fig. 2.** (a) Magnetization vs. temperature in the ZFC and FC modes for CFO and CFO-Ag, (b) Hysteresis loops recorded at  $T = 50$  K in

the ZFC mode, (c) and (d) show the  $M_{\text{IRM}}(H)$  and  $M_{\text{DCD}}(H)$  curves measured at  $T = 50$  K. Insets in (c) and (d) show the irreversible susceptibilities  $\chi_{\text{IRR}}$ .

**Table 1. (Upper)** Mean particle size for CFO and CFO-Ag systems as derived from XRD data ( $\langle d_{\text{XRD}} \rangle$ ), from TEM micrographs ( $\langle d_{\text{TEM}} \rangle$ ), from SAXS analysis ( $\langle d_{\text{SAXS}} \rangle$ ) and CFO polydispersity ( $\sigma$ ). **(Lower)** The blocking temperature ( $T_{\text{B}}$ ), irreversible temperature ( $T_{\text{irr}}$ ) and effective anisotropy constant ( $K_{\text{eff}}$ ) for CFO compared to CFO-Ag.

Sample	$\langle d_{\text{XRD}} \rangle$ (nm)	$\langle d_{\text{TEM}} \rangle$ (nm)	$\langle d_{\text{SAXS}} \rangle$ (nm)	$\sigma$ (%)
CFO	$12.0 \pm 1.0$	$8.4 \pm 2.2$	$11 \pm 3$	$26 \pm 1$
CFO-Ag	CFO = $10.8 \pm 2.0$ Ag = $7.0 \pm 3.0$	$8.1 \pm 2.3$ $8.0 \pm 4.0$	$10 \pm 3$ $5 \pm 2$	$15 \pm 1$ -
Sample	$\langle T_{\text{B}} \rangle$ (K)	$\langle T_{\text{irr}} \rangle$ (K)	$10^6 \langle K_{\text{eff}} \rangle^{(a)}$ (erg/cm <sup>3</sup> )	$10^5 \langle K_{\text{eff}} \rangle^{(b)}$ (erg/cm <sup>3</sup> )
CFO	$270 \pm 3$	$>300$	3.6	4.6
CFO-Ag	$250 \pm 2$	280	3.2	9.3

**Note:** (a) values calculated using Stoner-Wohlfarth relation, and (b) values given in percentage (%) for the Vogel-Fulcher relation.

The temperature dependence of  $M$  vs  $H$  plot for CFO-Ag is given in ESI (Fig. S5) and revealed a smooth decrease of the recorded anomaly upon increasing the temperature, till the point in which was lost for temperatures higher than the blocking temperature  $\langle T_{\text{B}} \rangle$ . Furthermore, the low-field anomaly in the hysteresis loop remained present in the hetero-nanosystem even after half year of ageing at room temperature (ESI, Fig. S4). In order to gain further understanding of the magnetic interparticle interactions, we measured the dependence of remanent magnetization with isothermal remanent magnetization (IRM) and direct current demagnetization (DCD) modes. The  $M_{\text{IRM}}(H)$  and  $M_{\text{DCD}}(H)$  trends witnessed in neat CFO and CFO-Ag measured at 50 K, temperature well below their respective  $\langle T_{\text{B}} \rangle$ , are shown in Fig. 2c and Fig. 2d. Considering the scenario of non-interacting assembly of superparamagnetic (SPM) nanoparticles having uniaxial anisotropy, the energy barrier distribution of the system can be determined from the  $M_{\text{IRM}}$  and  $M_{\text{DCD}}$  trends, and can be expressed according to the Stoner-Wohlfarth relation,<sup>12-13</sup> given by Eq. (1),

$$m^{\text{DCD}}(H) = 1 - 2m^{\text{IRM}}(H) \quad (\text{Eq. 1})$$

where the indexes  $m^{\text{DCD}}(H)$  and  $m^{\text{IRM}}(H)$  correspond to the reduced terms  $M^{\text{DCD}}(H)/M_{\text{S}}^{\text{DCD}}$  and  $M^{\text{IRM}}(H)/M_{\text{S}}^{\text{IRM}}$  respectively. Here, the  $M_{\text{S}}^{\text{DCD}}$  and  $M_{\text{S}}^{\text{IRM}}$  represent the remanence saturation values for the DCD and IRM plots. From the Stoner-Wohlfarth relation, the irreversible susceptibility  $\chi_{\text{IRR}} = dm/dH$  can be correlated to the IRM data using Eq. (2)<sup>13</sup>

$$|dm_{\text{DCD}}/dH| = 2(dm_{\text{IRM}}/dH) \quad (\text{Eq. 2})$$

with maxima located at the same reverse field. Any deviation witnessed from the expected trend anticipated by the Stoner-Wohlfarth model is considered to arise from interparticle interactions. In addition, these through-space interactions can be

further quantified in terms of the so-called interaction field ( $H_{\text{INT}}$ ), with expression given in Eq. (3)<sup>13</sup>

$$H_{\text{INT}} = (H'_{\text{R}} - H_{\text{R}})/2 \quad (\text{Eq. 3})$$

Here,  $H'_{\text{R}}$  and  $H_{\text{R}}$  are values related to the maxima in the irreversible susceptibility plot. The calculated value for CFO gave  $H_{\text{INT}}$  of  $-0.74$  kOe, showing the presence of weak demagnetization interactions, whereas for CFO-Ag gave  $H_{\text{INT}}$  of  $-0.19$  kOe and  $-0.14$  kOe, demonstrating that the demagnetization interactions became here weaker. In particular, we found good agreement between the magnetization loops recorded for CFO-Ag at 50 K (Fig. 2b) and the IRM/DCD curves, which displayed a broad bump at  $H \sim 1$  kOe (Fig. 2d). This phenomenon became well resolved from the  $\chi_{\text{IRR}}$  data, showing two distributions for CFO-Ag (inset in Fig. 2d) and only one for CFO (inset in Fig. 2c). Above 10 kOe the magnetic data become nearly identical in both CFO and CFO-Ag samples (insets Fig. 2c-d). Therefore once entered in the *blocked* regime of static magnetic experiments, the inclusion of Ag NPs within the CFO matrix led to the formation of a softer magnetic material. Here, the presence of metallic Ag seems capable of altering the overall system magnetic anisotropy. Interestingly, the magnetic dynamic trends displayed a different behaviour from the one observed under static regime. Fig. 3a-b show the  $T$ -dependence witnessed for the real  $\chi'(T)$  and imaginary  $\chi''(T)$  part of the susceptibility in CFO (Fig. 3a) and CFO-Ag (Fig. 3b) under a field  $H_{\text{ac}}$  of 5 Oe ( $50 \text{ K} < T < 350 \text{ K}$ ).

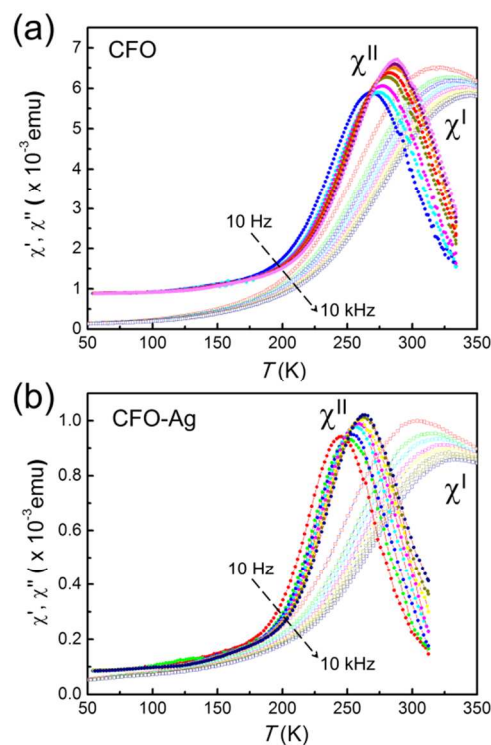


**Fig. 3.** Panel (a) and (b) show the  $T$ -dependence of the real ( $\chi'$ , open squares) and imaginary ( $\chi''$ , close circles) component of the ac susceptibility for CFO (panel a) and CFO-Ag (panel b) under an external field  $H_{\text{ac}}$  of 5 Oe.

The expected behaviour of blocking processes became evident, *i.e.* the occurrence of a maximum at  $T_B$ , which shifted towards higher temperatures and decreased in height with increasing frequency.<sup>14</sup> Such effect, visible upon sample cooling, is directly related to the frequency dependence of  $T_B$  from single-domain particles.<sup>12,14</sup> Looking at the  $\chi'(T)$  data of CFO and CFO-Ag, the observed peaks in these systems fall at similar temperatures. Two empirical relations, the Eq.(4) and Eq.(5) reported below, are often used in literature in way to compare the frequency dependence of  $T_B$  witnessed for various systems,

$$C_1 = \Delta T_B / T_B \Delta \log_{10}(f) \quad (\text{Eq. 4})$$

$$C_2 = (T_B - T_0) / T_B \quad (\text{Eq. 5})$$

The Eq. (4) is independent of any model. The terms  $\Delta T_B$  represents the difference between the  $T_B$  measured in the  $\Delta \log_{10}(f)$  frequency interval where  $f$  is the ac magnetic field frequency.<sup>14</sup> The parameters  $C_1$ ,  $C_2$  and  $T_0$  taken together deliver a model-independent classification of the blocking/freezing process.<sup>12-15</sup> However, it is important to note that Eq.(5) is a phenomenological relation and has no physical significance near  $T_0$ . Nevertheless,  $C_2$  can be taken as good indicator that screens different  $T_B$  in closely related materials. The variations of  $T_B$  in the classical plot of  $\log_{10}(\tau)$  vs.  $1/T_B$  for both CFO and CFO-Ag are given in the supporting material (ESI) as Fig. S6(c) (CFO) and Fig. S6(d) (CFO-Ag). For isolated nanoparticles, the  $f$ -dependence of  $T_B$  has been predicted, according to the SPM Neel model, to follow the Arrhenius law,  $\ln(\tau/\tau_0) = E_B/kT_B$ , where  $\tau = 1/f$ ,  $\tau_0$  represents the characteristic relaxation time constant ( $10^{-9}$  s  $< \tau_0 < 10^{-12}$  s), and  $E_B$  is the energy barrier of the NPs for the moment reversal.<sup>11</sup> Thus,  $E_B = KV$ , and  $K$  gives the effective anisotropy constant, with  $V$  the volume of the particle. The terms  $E_B$  and  $K$  were estimated from analyses of the experimental data. Even though a good fitting of the data has been obtained upon using the Arrhenius law for both CFO ( $E_B/k_B = 17926$  K,  $\tau_0 = 10^{-26}$  s) and CFO-Ag ( $E_B/k_B = 14687$  K,  $\tau_0 = 10^{-23}$  s), the results had no physical meanings. In particular, the  $\tau_0$  values were found much smaller than those physically accepted ( $10^{-26}$  s for CFO and  $10^{-23}$  s for CFO-Ag system), and  $E_B$  values were also found too high as compared to the reference values for  $\text{CoFe}_2\text{O}_4$  where  $E_B = 6925$  K (calculated using  $K = 2 \times 10^6$  erg/cm<sup>3</sup>). Thus, the experimentally observed variations in  $\chi'(T)$  for these samples were not consistent with the simple SPM blocking behaviour of independent particles. The data were then analysed by using the Vogel-Fulcher law,<sup>14</sup> relation that is written in the form of  $\tau = \tau_0 \exp \{E_A/k_B(T_B - T_0)\}$ . Here,  $T_0$  is an effective temperature with similar origin to that used to reproduce the dc susceptibility in the SPM regime and  $T_B$  is the characteristics temperature signalling the onset of the blocking process. Using the Vogel-Fulcher relation (ESI, Fig. 4d), the calculated fitted parameters became for CFO ( $E_B/k_B = 876$  K,  $\tau_0 = 10^{-8}$  s,  $T_0 = 256$  K) and CFO-Ag ( $E_B/k_B = 1846$  K,  $\tau_0 = 10^{-9}$  s,  $T_0 = 201$  K). These results give more reasonable values for  $\tau_0$  and  $E_B$ , and  $\tau_0$  and  $E_B$  becomes now comparable to those observed for spin-glass (SG) systems.<sup>14</sup> Notably, the analysis reveals that for CFO-Ag the energy barrier ( $E_B/k_B$ ) is enhanced at least twice in comparison to CFO, together

with a decrease in the effective temperature ( $T_0 = 201$  K for CFO-Ag,  $T_0 = 256$  K for CFO). From the results obtained in the static and dynamic magnetic behaviour of CFO-Ag we can therefore conclude that under dc or low ac fields, the presence of Ag NPs enhances the magnetic relaxation of bulk CFO-Ag hetero-composite, phenomenon that leads to weakening the magnetocrystalline anisotropy. On the contrary, when CFO-Ag is exposed to high frequencies of ac fields, damping effects emerge in its relaxation behaviour. Since the effect being observed is associated to the collective behaviour of the material, we attempted to dissect in more depth the saturation behaviour using micromagnetic simulations (MMS), in order to gain deeper understanding of the low-field anomaly witnessed in the hetero-nanosystem. The results are presented in Fig. 4a-c. The CFO NPs were modelled as single homogeneous nanoparticles, with diameter of  $\sim 10$  nm, using  $A \sim 30 \times 10^{12}$  A/m,  $M_s \sim 1400 \times 10^3$  J/m and uniaxial anisotropy  $K \sim 900 \times 10^3$  J/m<sup>3</sup>. Locally, the CFO-Ag system was modelled according to a core plus shell architecture, made by those CFO NPs that are more tightly interacting with Ag (core) and the remaining CFO that are weakly interacting with Ag (shell). Although this model represents clearly a simplified picture of the real system, it finds reasoning from the witnessed double distribution obtained from the  $\chi_{\text{IRR}}$  measurements (see Fig. 2c and Fig. 2d) as well as from the HRTEM imaging, Mössbauer and SAXS data. For the core (CFO-Ag) we used the same parameters  $A$ ,  $K$  and  $M_s$  as mentioned above with an approximate diameter of  $\sim 9$  nm, while for the interacting shell (CFO) we employed in the simulation a 3 nm thickness and slightly lower values, namely for  $A \sim 9 \times 10^{12}$  A/m,  $M_s \sim 200 \times 10^3$  J/m, and  $K \sim 5.7 \times 10^2$  J/m<sup>3</sup>.

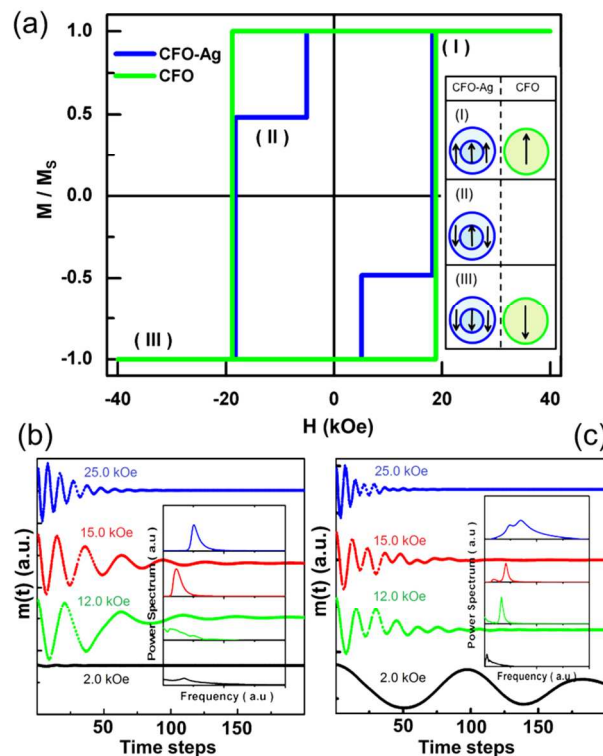


**Fig. 4.** (a) Calculated hysteresis loops for CFO-Ag and neat CFO along with their schematic representation of the magnetization

reversal processes. Magnetic relaxation of the normalized magnetization ( $M/M_S$ ) against time steps for (b) homogeneous spherical CFO and (c) CFO-Ag sample. Insets show the respective Fourier-transform (FFT) spectra.

In both scenarios (neat CFO and CFO-Ag), the damping parameter was set to 0.5 in the static simulations and interparticle interactions were neglected. The calculated hysteresis cycle in the case of CFO exhibited a squared loop shape (Stage I and Stage III), signature that becomes softened when interparticle interactions are active.<sup>16</sup> On the contrary, for the CFO-Ag, the calculated magnetization reversal was found to consist of one additional stage (Fig. 4a, blue line, Stage I, II and III). Here, the intermediate step, Stage II, in the hysteresis loop represents the material's region in which the magnetization is not yet flipped contrary to the bulk CFO. This portion of material is composed, in our assumption, by the CFO nanoparticles in close contact with Ag. Upon increasing the magnetic field, this core magnetization reverses in line with the shell. To understand the dynamics of these systems, we used an oscillating magnetic field<sup>17-19</sup>,  $H_{ac}(t)$  with rise time of 1000  $\mu$ s and peak amplitude of 5 Oe along the anisotropy direction, and different values for the bias field,  $H_{bias} \sim 1 - 25$  kOe, applied perpendicular to the ac field. Fig. 4b and Fig. 4c illustrate the magnetic relaxation,  $m(t)$  for CFO (Fig. 4b) and CFO-Ag (Fig. 4c) samples. We found that for CFO there is no relaxation for fields lower than 5.0 kOe, whereas for CFO-Ag, relaxation persists even for  $H_{bias} \sim 2.0$  kOe. Furthermore, in CFO-Ag two oscillations modes emerged, one corresponds to the core and the other arising from the shell. The insets in Fig. 4b-4c depict the Fast Fourier Transform of the data, showing for the CFO particles no maxima for  $H_{bias}$  less than 12.0 kOe, and no uniform precession at low magnetic fields occurs due to the hardness of the particle. On the contrary, for CFO-Ag a maximum for all simulations has been found, showing that even at low fields there is precession of the magnetization around  $H_{bias}$ . This is due to the presence of Ag NPs in the CFO matrix, which is capable to modulate the magnetization precession in fields as low as  $\sim 2.0$  kOe. In conclusion, we observed that the magnetic relaxation mechanisms of  $CoFe_2O_4$  nanoparticles is strongly affected by inclusion of non-magnetic Ag nano-counterparts, behaviour that departed from the well-known scenario described by the SPM Stoner-Wohlfarth model. The observed changes in the magnetic relaxation behaviour of CFO-Ag arise from damping effects, probably due to the hybridization of  $CoFe_2O_4$  and Ag electronic structures. In contrast to  $CoFe_2O_4$ , the CFO-Ag nano-system showed a remarkable enhancement in the effective energy barrier. This work can therefore open novel opportunities for designing other hetero nanosystems in which the relaxation behaviour and effective barriers can be tuned by nonmagnetic counterparts. Furthermore, our findings may inspire assembly of less conventional hetero-systems architectures based on e.g. single molecule magnets (SMM) for the emerging field of molecular data-storage devices.

## Notes and references

<sup>1</sup>Instituto de Física Gleb Wataghin, Universidade Estadual de Campinas (UNICAMP) Campinas, 13.083-859, SP, Brazil.  
E-mail: [surender76@gmail.com](mailto:surender76@gmail.com), [knobel@ifi.unicamp.br](mailto:knobel@ifi.unicamp.br)

<sup>2</sup>Laboratoire Interfaces Traitements Organisation et Dynamique des Systemes (ITODYS), UMR 7086 CNRS & Universite Paris Diderot-Paris 7, Case 7090, 75205 Paris, Cedex 13, France

<sup>3</sup>Regional Centre of Advanced Technologies and Materials, Faculty of Science, Palacký University Olomouc, 771 46 Olomouc, Czech Republic

<sup>4</sup>Advanced Materials Research Institute, University of New Orleans, New Orleans, Louisiana 70148, USA

<sup>5</sup>Physics Department, Universidad de Santiago de Chile and CEDENNA, USACH, Santiago 917-0124, Chile

† Authors from UNICAMP are very grateful to CNPq and FAPESP (Brazil). Authors from Czech Republic acknowledge research support from the project LO1305 of the Ministry of Education, Youth and Sports of the Czech Republic. In Chile, we acknowledge support from FONDECYT under grant 1120356, CONICYT, Grant ICM P10-061-F by FIC- MINECON, CEDENNA and AFOSR Grant FA9550-11-1-0347. The authors sincerely thank Dr. Jiri Tucek (Regional Centre of Advanced Technologies and Materials, Czech Republic) for carrying out the Mössbauer experiments and analysis.

Electronic Supplementary Information (ESI) available: [Experimental details, characterization techniques, XRD, Mössbauer, SAXS data, additional  $M$  vs  $H$  plots and Arrhenius and Vogel-Fulcher plots]. See DOI: 10.1039/c000000x/

1 (a) Y. Li, Q. Zhang, A. V. Nurmikko, and S. Sun, *Nano Lett.* 2005, **5**, 1689; (b) F. Pineider, C. de J. Fernandez, V. Videtta, E. Carlino, Awni al Hourani, F. Wilhelm, A. Rogalev, P. Davide Cozzoli, P. Ghigna and C. Sangregorio, *ACS Nano* 2013, **7**, 857.

2 (a) Y. D. Jin, C. Jia, S. -W. Huang, M. O'Donnell, X. Gao, *Nat. Commun.* 2010, **1**, 41; (b) S.H. Choi, H. B. Na, Y. I. Park, K. An, S. G. Kwon, Y. Jang, M. H. Park, J. Moon, J. S. Son, I. C. Song, W. K. Moon, T. Hyeon, *J. Am. Chem. Soc.* 2008, **130**, 15573; (c) Y. Zhai, L. Han, P. Wang, G. Li, W. Ren, L. Liu, E. Wang, and S. Dong, *ACS Nano* 2011, **5**, 8562; (d) J. Xie, F. Zhang, M. Aronova, L. i Zhu, X. Lin, Q. Quan, G. Liu, G. Zhang, K.-Y. Choi, K. Kim, X. Sun, S. Lee, S. Sun, R. Leapman, X. Chen, *ACS Nano* 2011, **5**, 3043; (e) M. Casavola, A. Falqui, M. A. García, M. G. - Hernández, C. Giannini, R. Cingolani, and P. Davide Cozzoli, *Nano Lett.* 2009, **9**, 366.

3 (a) C. Wang, H. Yin, S. Dai, and S. Sun, *Chem. Mater.* 2010, **22**, 3277; (b) F.-h. Lin, and R.-an Doong, *J. Phys. Chem. C* 2011, **115**, 6591; (c) J.-S. Choi, Y.-W. Jun, S.-In Yeon, H. C. Kim, J.-S. Shim, J. Cheon, *J. Am. Chem. Soc.* 2006, **128**, 15982.

4 X. Liu, R. P. Panguluri, Z. F. Huang, and B. Nadgorny, *Phys. Rev. Lett.* 2010, **104**, 035701.

5 Z. Xu, Y. Hou, S. Sun, *J. Am. Chem. Soc.* 2007, **129**, 8698.

6 (a) B. Lim, J. Wang, P. H. C. Camargo, M. Jiang, M. J. Kim, and Y. Xia, *Nano Lett.* 2008, **8**, 2535; (b) M. Sytnyk, R. Kirchschrager, M. I. Bodnarchuk, D. Primetzhofer, D. Krieger, H. Enser, J. Stangl, P. Bauer, M. Voith, A. W. Hassel, F. Krumeich, F. Ludwig, A. Meingast, G. Kothleitner, M. V. Kovalenko, W. Heiss, *Nano Lett.* 2013, **13**, 586.

7 Y. Sun, Y. Xia, *Science* 2002, **298**, 2176.

8 Y. K. Mishra, S. Mohapatra, D. Kabiraj, B. Mohanta, N.P. Lalla, J.C. Pivin, D.K. Avasthi, *Scripta Materialia* 2007, **56**, 629.

9 G. Lopes, J. M. Vargas, S. K. Sharma, F. Béron, K. R. Pirota, M. Knobel, C. Rettori, R. D. Zysler, *J. Phys. Chem. C* 2010, **114**, 10148.

10 J. M. Vargas, A. A. McBride, J. B. Plumley, Y. Fichou, T. A. Memon, V. Shah, N. C. Cook, B. A. Akins, A. C. Rivera, G. A. Smolyakov, J. R. O'Brien, N. L. Adolphi, H. D. C. Smyth, M. Osiński, *J. Appl. Phys.* 2011, **109**, 07B536.

11 S. K. Sharma, G. Lopes, J. M. Vargas, L. Socolovsky, K. R. Pirota, and M. Knobel, *J. Appl. Phys.* 2011, **109**, 07B530.

12 M. Knobel, W. C. Nunes, L. M. Socolovsky, E. De. Biasi, J. M. Vargas, J. C. Denardin, *J. Nanosci. Nanotechnol.* 2008, **8**, 2836.

13 (a) E. C. Stoner, E. P. Wohlfarth, *Phyl. Trans. Royal Soc. A* 1948, **240**, 599. (b), E. P. Wohlfarth, *J. Appl. Phys.* 1958, **29**, 595. (c) J. L. Dormann, L. Bessais, and D. Fiorani, *J. Phys. C: Solid State Phys.* 1998, **21**, 2015.

14 (a) J. M. Vargas, A. Srivastava, A. Yourdkhani, L. Zaldivar, G. Caruntu, and L. Spinu, *J. Appl. Phys.* 2011, **110**, 064304; (b) S. K. Sharma, R. Kumar, S. Kumar, M. Knobel, C. T. Meneses, V. V. Siva Kumar, V. R. Reddy, M. Singh, C. G. Lee, *J. Phys. Condens. Matter* 2008, **20**, 235214.

15 J. L. Dormann, D. Fiorani, E. Tronc, *J. Magn. Magn. Mater.* 1999, **202**, 251.

- 16 M. Bahiana, F. Amaral, S. Allende, and D. Altbir, *Phys. Rev. B* 2006, **74**, 174412.
- 17 A. Barman, S. Barman, *Phys. Rev. B* 2009, **79**, 144415.
- 18 S. Pal, D. Kumar, A. Barman, *J. Phys. D: Applied Physics* 2011, **44**, 105002.
- 19 S. Saha, R. Mandal, S. Barman, D. Kumar, B. Rana, Y. Fukuma, S. Sugimoto, Y. C. Otani, A. Barman, *Adv. Funct. Mater.* 2013, **23**, 2378.

## Table of Content TOC

**Synopsis:** The analysis of static and dynamic magnetic response of  $\text{CoFe}_2\text{O}_4$ -Ag hetero nano-system revealed, with the aid of micromagnetic simulations, a severe alteration of the magnetic relaxation behaviour of  $\text{CoFe}_2\text{O}_4$  upon interaction with non-magnetic Ag.

